STEM CELLS®

TRANSLATIONAL AND CLINICAL RESEARCH

Direct Evidence of Mesenchymal Stem Cell Tropism for Tumor and Wounding Microenvironments Using In Vivo Bioluminescent Imaging

SHANNON KIDD,[a] ERIKA SPAETH,[a] JENNIFER L. DEMBINSKI,[a] MARTIN DIETRICH,[a] KERI WATSON,[a] ANN KLOPP,[b] VENKATA LOKESH BATTULA,[a] MICHEAL WEIL,[a] MICHAEL ANDREEFF,[a] FRANK C. MARINI[a]

[a]Section of Molecular Hematology and Therapy, Department of Stem Cell Transplantation and Cellular Therapy and [b]Dept of Radiation Oncology, University of Texas M.D. Anderson Cancer Center, Houston, Texas, USA

Key Words. Mesenchymal stem cell • Tumor tropism • Inflammatory microenvironment • Bioluminescent imaging

ABSTRACT

Multipotent mesenchymal stromal/stem cells (MSC) have shown potential clinical utility. However, previous assessments of MSC behavior in recipients have relied on visual detection in host tissue following sacrifice, failing to monitor in vivo MSC dispersion in a single animal and limiting the number of variables that can be observed concurrently. In this study, we used noninvasive, in vivo bioluminescent imaging to determine conditions under which MSC selectively engraft in sites of inflammation. MSC modified to express firefly luciferase (ffLuc-MSC) were injected into healthy mice or mice bearing inflammatory insults, and MSC localization was followed with bioluminescent imaging. The inflammatory insults investigated included cutaneous needle-stick and surgical incision wounds, as well as xenogeneic and syngeneic tumors. We also compared tumor models in which MSC were i.v. or i.p. delivered. Our results demonstrate that ffLuc-expressing human MSC (hMSC) systemically delivered to nontumor-bearing animals initially reside in the lungs, then egress to the liver and spleen, and decrease in signal over time. However, hMSC in wounded mice engraft and remain detectable only at injured sites. Similarly, in syngeneic and xenogeneic breast carcinoma-bearing mice, bioluminescent detection of systemically delivered MSC revealed persistent, specific colocalization with sites of tumor development. This pattern of tropism was also observed in an ovarian tumor model in which MSC were i.p. injected. In this study, we identified conditions under which MSC tropism and selective engraftment in sites of inflammation can be monitored by bioluminescent imaging over time. Importantly, these consistent findings were independent of tumor type, immunocompetence, and route of MSC delivery. STEM CELLS *2009;27:2614–2623*

Disclosure of potential conflicts of interest is found at the end of this article.

INTRODUCTION

Multipotent mesenchymal stromal cells (MSC), also referred to as mesenchymal stem cells, have demonstrated preferential incorporation into sites of tumor development [1, 2] and injury [3–5]. This selective integration has been attributed to the high levels of inflammatory mediators produced in the associated microenvironment [6]. Tissues confronted with acute insults involve states of injury that exhibit an array of inflammatory chemotactic molecules to which MSC respond [6]. Such states include: (a) hypoxia or ischemia [7–10], a state of reduced oxygen that often parallels and perpetuates inflammation; (b) radiation, used as therapy or as a weapon [11–13]; (c) tumors, which mimic the phenotype of an "unhealed wound" [14]; and (d) cutaneous cuts or punctures that delineate the conventional definition of inflammation [15]. Exploitation of this MSC tropism offers numerous therapeutic applications for an array of disorders, including myocardial infarction [16–18], muscular dystrophy [19], osteogenesis imperfecta [20], spinal cord injury [21], graft-versus-host disease [22], and cancer [1, 2]. Despite the great therapeutic potential, unanswered questions remain regarding homing, engraftment, and safety of the transplanted stem cells [23].

In animal experiments, labeled MSC can be monitored by immunohistochemical (IHC) staining [11], fluorescent visualization [24], or DNA polymerase chain reaction (PCR) [25, 26] to examine the migratory endpoint of these labeled cells only after the animal has been sacrificed. Although sensitive, these methods require the use of numerous animals to be sacrificed at multiple time points and allow the opportunity for sampling limitations to occur when only certain parts of the tissue or organ are harvested and analyzed. To circumvent single time point experiments, we have employed in vivo bioluminescent imaging. This method detects visible light produced when cells modified to express reporter enzymes, such

Author contributions: S.K.: conception and design, collection and assembly of data, data analysis and interpretation, manuscript writing; E.S.: conception and design, data analysis and interpretation, manuscript writing; J.L.D.: conception and design, collection and assembly of data, data analysis and interpretation; M.D.: collection and assembly of data, provision of study material; K.W.: collection and assembly of data; A.K.: collection and assembly of data; L.B.: collection and assembly of data; M.W.: provision of study material; M.A.: conception and design, financial support; F.C.M.: conception and design, data analysis and interpretation, financial support, final approval of manuscript.

Correspondence: Frank C. Marini, Ph.D., Stem Cell Transplant and Cellular Therapy, Box 081, M.D. Anderson Cancer Center, 1515 Holcombe Boulevard, Houston, Texas 77030, USA. Telephone: 713-794-5644; Fax: 713-794-4747; e-mail: fmarini@mdanderson.org Received January 14, 2009; accepted for publication July 22, 2009; first published online in STEM CELLS *EXPRESS* July 30, 2009. 1066-5099/2009/$30.00/0 doi: 10.1002/stem.187

as firefly luciferase (ffLuc), react with their specific bioluminescent substrates [27], and allows for noninvasive, serial detection of these cells in vivo [28, 29]. Though visible light is limited in depth of tissue penetration, the technique is ideal and cost-effective for imaging small animals such as mice. Additionally, multiple labeled cell populations can be detected in the same animal, affording the use of significantly fewer animals than previous methods. Furthermore, these reporter enzymes are only expressed in viable, metabolically active cells [30]. Bioluminescent imaging has already facilitated the study of tumor growth and response to treatments [31, 32], gene expression in cells [29], the trafficking of lymphocytes in vivo [33], and hematopoietic stem cell engraftment in host tissues [34, 35]. This method has also been used to image MSC injected into myocardium [36–38], models of acute kidney injury [39], and s.c. transplanted ceramic cubes [40] and scaffolds [41].

We show herein that bioluminescent imaging can reveal dynamic information detailing the distribution and tropism of MSC in host tissues toward inflammatory tumor and wound microenvironments. We demonstrate the biodistribution of systemically injected human MSC (hMSC) in nontumor-bearing severe combined immunodeficient (SCID) mice, wherein hMSC initially distribute to the lungs, liver, and spleen and then diminish in bioluminescent signal until they are undetectable at 14 days. We then show specific colocalization of injected hMSC in two different cutaneous wounding events. Next, we followed MSC in tumor-bearing SCID mice and found selective MSC engraftment at the site(s) of tumor development when MSC were delivered by i.v. or i.p. administration. Finally, similar results were seen in an immunocompetent, syngeneic Balb/C breast tumor model in which murine MSC (mMSC) specifically colocalized with s.c. established tumors. Regardless of immunocompetence or route of MSC administration, bioluminescent imaging revealed specific tropism and engraftment of MSC in all tumor and wounding models investigated, indicating that MSC could be useful biodetectors of these disease states.

Materials and Methods

Isolation and Expansion of hMSC and mMSC

hMSC were isolated from the bone marrow of normal individuals undergoing bone marrow harvest for allogeneic bone marrow transplantation following informed consent, according to institutional guidelines under the approved protocol, as described previously [2]. Briefly, mononuclear cells were separated by centrifugation over a Ficoll-Hypaque gradient (Sigma-Aldrich, St. Louis, http://www.sigmaaldrich.com), suspended in 10 ml of MSC complete medium—α-minimum essential medium (α-MEM) containing 20% fetal bovine serum (FBS) (Invitrogen, Carlsbad, CA, http://www.invitrogen.com), L-glutamine, and penicillin–streptomycin mixture (Gibco/Invitrogen)—and plated on 180-cm^2 dishes. After 3 days, nonadherent cells were removed by washing with phosphate-buffered saline (PBS), and monolayers of adherent cells were cultured until they reached confluence. Cells were then trypsinized (0.25% trypsin with 0.1% EDTA) and subcultured at densities of 5,000–6,000 cells/cm^2. Cell passages 3–4 were used for the experiments.

mMSC were isolated as described previously [42]. Briefly, femurs of 2-month-old Balb/C (Harlan Laboratories, Inc., Indianapolis, IN, http://www.harlan.com) mice were collected, dissected into small fragments, then placed into a sterile mortar and crushed using a sterile pestle. Whole bone fragments and bone marrow pieces were then placed in toto into 10 ml MSC complete medium and plated on 180-cm^2 dishes. After 5 days, plates were washed to remove nonadherent cells. After two complete washings, adherent cells were retrieved by trypsinization and immunodepleted of granulomonocytic cells using a biotinylated antibody against CD11b (BD Biosciences, San Jose, CA, http://www.bdbiosciences.com) and streptavidin-coated microbeads from Miltenyi Biotec (Auburn, CA, http://www.miltenyibiotec.com), according to the manufacturer's instructions. After immunodepletion, the remaining cells were plated in fresh medium, and within an additional 3 days, fibroblast-like colonies were observed. The medium was changed two to three times per week and cell density was maintained at 2,000–6,000 cells/cm^2.

To determine the multilineage differentiation potential of hMSC, we subjected passage 3 hMSC to various differentiation media, according to the manufacturer's recommendations (Miltenyi Biotec). Briefly, hMSC were cultured for 3 weeks in NH AdipoDiff, NH OsteoDiff, or ChondroDiff medium with medium changes ever 3 days. Adipocytes were then stained with oil red O (Sigma), and osteoblasts were stained for calcium with Alizarin red S. For chondrogenic detection, hMSC pellets were sectioned and stained with Alcian blue. ffLuc-MSC were also assayed for their adiopgenic, osteogenic, and chondrogenic potentials.

Cell Culture

Human MDA-MB-231 breast cancer cells (a generous gift from Dr. I. Fidler, M.D. Anderson Cancer Center, Houston, TX), were maintained in α-MEM containing 10% FBS, sodium pyruvate, nonessential amino acids, L-glutamine, vitamin solution (Life Technologies, Grand Island, NY, http://www.lifetech.com), and penicillin–streptomycin mixture. Human ovarian cancer HEY cells and murine breast carcinoma 4T1 cells were obtained from American Type Culture Collection (Manassas, VA, http://www.atcc.org) and cultured in Roswell Park Memorial Institute medium (RPMI-1640) supplemented with 10% fetal calf serum and penicillin–streptomycin mixture. Murine 4T1 cells were stably transduced with a lentivirus expressing renilla luciferase (4T1-rLuc), as described previously [42].

Flow Cytometry

MSC were harvested with 0.25% trypsin-EDTA and resuspended in PBS supplemented with 2% FBS. Approximately 1×10^6 cells were stained with 1 μg of antibody for 30 minutes at 4°C, and then analyzed on a fluorescence-activated cell sorting (FACS)Caliber flow cytometer (Becton, Dickinson and Company, Franklin Lakes, NJ, http://www.bd.com). The human antibodies used included CD105, CD90, CD140b, CD73, CD166, CD44, CD146, CD31, and CD34 (BD Biosciences). Antibodies specific for mouse antigens included Sca-1, CD106, CD140b, CD44, CD31, CD11b and CD45 (eBioscience, San Diego, http://www.ebioscience.com).

Adenoviral Vector and MSC Transduction

A recombinant adenoviral (Ad) vector expressing ffLuc, possessing an RGD-modified fiber (AdLuc-F/RGD) was prepared, purified, and titered as described previously [43]. hMSC were incubated with AdLuc-F/RGD at 3,000 viral particles per cell (vp/cell) (based on optical density reading) for 4 hours, while Balb/C and C57Bl/6 MSC were incubated with AdLuc-F/RGD at 5,000 vp/cells for 6 hours in serum-free medium. After incubation, serum-containing medium was added to the culture. The transduction efficiency was routinely >95% in both hMSC and mMSC, as previously reported [43]. MSC were assessed for luciferase expression by plating 5×10^4 transduced MSC into 24-well plates and adding 1 μl of D-Luciferin (40 mg/ml stock) (Caliper Life Sciences, Inc., Hopkinton, MA) into 2 ml culture medium. Thirty seconds later, cells were placed into the imager for detection. Using this multiplicity of infection protocol, we routinely detected >500 copies of Ad-delivered ffLuc transcript/MSC by quantitative reverse transcription PCR, and bioluminescence could be detected for up to 30 days (data not shown). A single transfection was performed at each time point to provide all

animals in the same experiment with the same source of donor MSC.

Animals

Female Balb/C and SCID/CB-17 mice were purchased from Jackson Laboratory (Bar Harbor, ME, http://www.jax.org). Mice were used in accordance with institutional guidelines under the approved protocols.

s.c. Detection of MSC In Vivo

Cell doses in the range of 10–300 ffLuc-MSC were injected s.c. in 10 μl PBS ($n = 3$). A control animal was injected with PBS alone. Immediately postinjection, ffLuc-hMSC bioluminescence was detected and imaged with a Xenogen IVIS imaging system (Caliper Life Sciences) after substrate administration.

MSC Administration to Nontumor-Bearing Animals

ffLuc-hMSC (1×10^6) suspended in 100 μl PBS were injected into the tail vein of SCID mice ($n = 5$). The mice were imaged for bioluminescence detection to pinpoint ffLuc-hMSC location at 1, 3, 5, 7, and 10 days after MSC injection. Likewise, 1×10^6 ffLuc-mMSC generated from a Balb/C mouse, suspended in 100 μl PBS, were i.v. injected via the tail vein in syngeneic Balb/C mice ($n = 5$). These mice were imaged 1.5, 2.5, 10, 18, and 24 hours after ffLuc-mMSC injection.

Cutaneous Wounding Models and MSC Administration

Anesthetized SCID mice were shaved and cleaned with sterile alcohol and gauze. A s.c. surgical incision (1.25 cm) was made on the right side of the abdomen ($n = 3$). This incision was immediately sutured shut with five stitches, and the mouse was isolated in a private cage. Three days postsurgery, the mice were injected via the tail vein with 2.5×10^5 ffLuc-hMSC. The tail vein puncture wounding experiments were done on mice receiving three separate injections using a 27-gauge needle along the lateral tail vein during the injection of 2.5×10^5 ffLuc-MSC ($n = 5$). All wounded mice were imaged over a period of 2 weeks, at which time point they were sacrificed.

Tumor Models and MSC Administration

Xenograft Tumors. MDA-MB-231 cells (5×10^5) in 100 μl of PBS were administered i.v. via the tail vein of SCID mice and allowed to seed the lungs ($n = 5$). After 10 days, 1×10^6 ffLuc-hMSC were i.v. injected in 100 μl PBS. ffLuc-hMSC localization was tracked by bioluminescent imaging twice per week until sacrifice of the animals at day 29. HEY ovarian carcinoma cells (5×10^5) were suspended in 1 ml PBS and i.p. injected into SCID mice ($n = 3$). Fifteen days after tumor injection, 1×10^6 ffLuc-hMSC were i.p. injected in 100 μl PBS, and these cells were monitored three times per week for 2 weeks, at which time point these animals were sacrificed.

Syngeneic Tumors. Balb/C derived murine 4T1 breast carcinoma cells (2.5×10^5) were s.c. injected into the hind limbs of Balb/C mice. After 10 days of tumor establishment, 1×10^6 ffLuc-mMSC were i.v. injected, as described previously, and followed by imaging two times per week until sacrifice at 12 days. See supporting information Table 1, which details the experimental design of the tumor models. In all experiments, mice were allowed to recover for 1 hour before being placed into group cages after injection.

Bioluminescent Imaging

In vivo optical imaging was performed with a Xenogen IVIS bioluminescence/fluorescence optical imaging system at different time points. Five minutes prior to imaging, each mouse was given a 100-μl i.p. injection of D-Luciferin (Caliper Life Sciences) at a dose of 125 mg/kg or a 100-μl injection of 40 mg/ml coelenterazine, as described previously [11]. General anesthesia was then induced with 5% isoflurane (IsoSol; Medeva Pharmaceuticals, Inc., Rochester, NY) and the mouse was placed in a light-tight heated chamber; anesthesia was continued during the procedure with 2% isoflurane introduced via a nose cone. The imaging system consists of a cooled, back-thinned, charge-coupled device (CCD) camera to capture both a visible light photograph of the animal taken with light-emitting diodes and the luminescent image. After acquiring photographic images of each mouse, anterior and posterior luminescent images were acquired with 1- to 3-minute exposure times. The resulting gray scale photographic and pseudocolor luminescent images were automatically superimposed so that identification of any optical signal with location on the mouse was facilitated. Optical images were displayed and analyzed with IVIS Living Image (Caliper Life Sciences) software packages. Regions were manually drawn around the bodies of the mice to assess the relative signal intensity emitted. Optical signal was expressed as photon intensity, in units of photons/second (p/s) within the region of interest.

Detection of MSC by IHC and Fluorescence

Tumors and other organs were fixed in Bouin's solution or embedded in OCT compound (Miles, Inc., Elkhart, IN) and then snap-frozen in liquid nitrogen and stored at -80°C. Frozen tissue was sectioned (6–8 μm) and processed for hematoxylin-eosin staining, IHC staining, or direct visualization. Imaging was performed with a Zeiss Axioplan2 microscope (Carl Zeiss Inc., Thornwood, NY, http://www.zeiss.com) equipped with a CCD camera (Hamamatsu Corp., Bridgewater, NJ, http://www.hamamatsu.com) and Adobe Photoshop software (Adobe Systems Inc., San Jose, CA, http://www.adobe.com).

IHC. Slides from frozen tissues were fixed with neutral buffered formalin (5 minutes), followed by 0.3% hydrogen peroxide in methanol (30 minutes) to quench endogenous peroxidase. Anti-ffLuc IHC was preformed using a 1:500 dilution (Promega, Madison, WI, http://www.promega.com). For primary antibody detection, the mouse ABC kit (Vector Laboratories, Burlingame, CA, http://www.vectorlabs.com) was used. Peroxidase substrate was developed using either the 3,3′-diaminobenzidine (DAB) or 3-amino-9-ethylcarbazole (AEC) substrate kit (Vector labs). Slides were counterstained with Hematoxylin QS (Vector labs) and mounted using either vectamount mounting medium, for DAB-stained slides (Vector labs), or aqueous mounting medium, for AEC-stained slides (ScyTek Laboratories, Logan, UT, http://www.scytek.com). For direct fluorescence visualization, MSC were labeled prior to transplantation with Sp-DiI (Molecular Probes, Carlsbad, CA, http://probes.invitrogen.com), as described previously [24].

Statistical Analysis

Numerical data are expressed as mean ± standard error. Statistical differences between the means for the different groups were evaluated with Prism 4.0 (GraphPad Software Inc., La Jolla, CA, http://www.graphpad.com) using either the Student's *t*-test or analysis of variance, with the level of significance at $p < .05$.

Results

Characterization of MSC

FACS analysis demonstrated that hMSC expressed high levels of CD105, CD90, CD140b, CD73, CD166, and CD44 and lower levels of CD146, in accord with accepted phenotypic markers for hMSC [44]. These cells did not express the endothelial marker CD31, the primitive hematopoietic marker CD34, or the mature hematopoietic marker CD45 (Fig. 1A). mMSC were verified to express CD44, CD106, CD140b, and

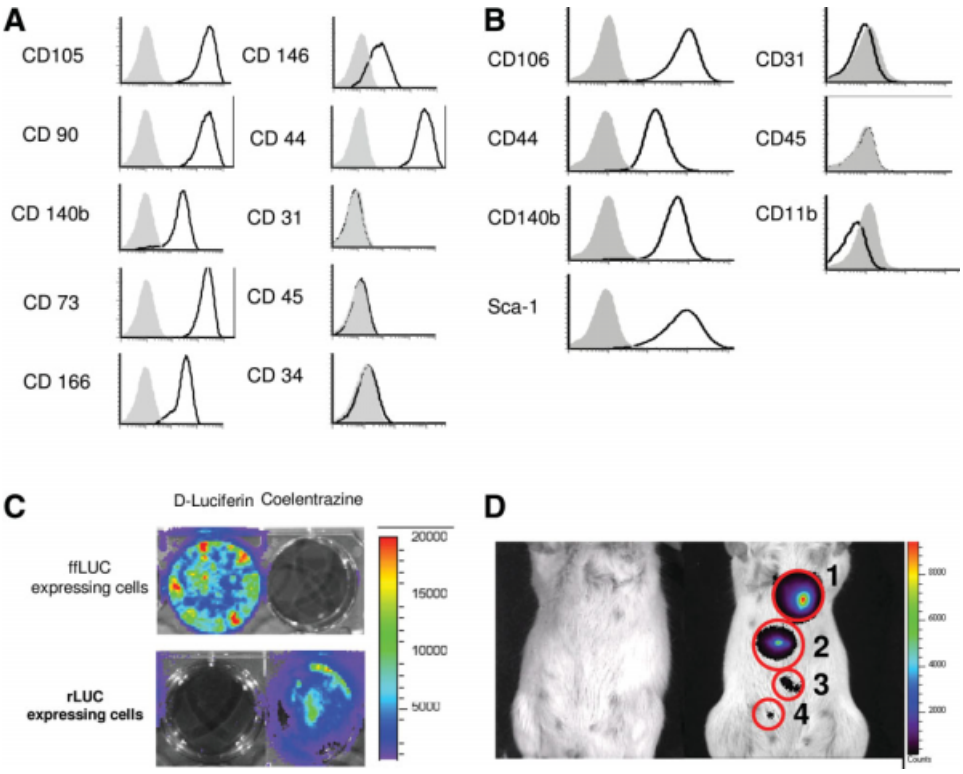

Figure 1. MSC characterization and labeling for in vivo visualization. hMSC**(A)** and mMSC **(B)** were evaluated for phenotypic markers by flow cytometry. **(C):** ffLuc-expressing and rLuc-expressing cells showed specific reactivity with D-Luciferin and coelentrazine, respectively. **(D):** In vivo detection of ffLuc-MSC was evaluated at 0 (far left mouse), 300 (1), 100 (2), 30 (3), and 10 (4) cells per s.c. injection. Increasing numbers of MSC demonstrated correlated increases in signal intensity. Abbreviations: ffLuc, firefly luciferase; hMSC, human MSC; mMSC, murine MSC; MSC, mesenchymal stromal cell; rLuc, renilla luciferase.

Sca-1. Similarly to the human cells, mMSC were also negative for the endothelial, macrophage/monocyte, and panhematopoietic markers CD31, CD11b, and CD45, respectively (Fig. 1B). These patterns of expression were consistent across all MSC used in the following experiments. Additionally, we subjected hMSC before and after ffLuc transduction to adipogenic, osteoblastic, and chondrogenic differentiation assays. In all cases oil red O^+, Alizarin red S^+, and Alcian $blue^+$ cells were detected after culture, suggesting that these cells maintained their differentiation potential regardless of adenoviral transduction (supporting information Fig. 1).

Level of Detection of ffLuc-MSC

Next, we demonstrated that the ffLuc substrate, D-Luciferin, displayed bioluminescent activity only when exposed to cells expressing ffLuc and not cells expressing renilla luciferase (rLuc). Likewise, the rLuc substrate, coelentrazine, was only active in cells expressing rLuc (Fig. 1C). To determine the sensitivity of our in vivo detection of MSC, we injected ffLuc-hMSC beneath the skin of SCID mice. As illustrated in Figure 1D, the control animal displayed no detectable bioluminescent activity, whereas 300, 100, 30, and 10 cells could be detected in animals receiving s.c. ffLuc-hMSC.

Biodistribution of MSC in Homeostatic SCID and Balb/C Recipients

To follow the biodistribution of hMSC in a homeostatic host, lacking an inflamed microenvironment, ffLuc-hMSC were i.v. injected into SCID mice. The mice were imaged for bioluminescence detection to pinpoint ffLuc-hMSC location over time. As seen in Figure 2A, mice imaged on the day of injection (day 1) showed intense signal, predominantly in the lungs. The dorsal view illustrates the presence of two distinct hot spots of activity, which correspond to the location of two lung lobes. The bioluminescent signal decreased by threefold and remained localized to the lung 3 days postinjection. However, at day 5, a small population was observed exiting the lungs and appearing in the liver (Fig. 2, day 5). By 7 days postinjection, ffLuc-hMSC activity in the lung was even further reduced, and most activity was localized to the liver and spleen (Fig. 2, day 7). Ten days after injection, ffLuc-hMSC activity remained in the liver and was undetectable in the lungs (Fig. 2, day 10). Photon counts of the lung region over time demonstrated a quantitative decrease from its initial peak of 21,710 $\pm$ 9,220 p/s on day 1, becoming undetectable by day 10 (Fig. 2B). Conversely, photon counts in the liver region were absent at the initial time point and slowly increased to their peak between day 7 (2,030 $\pm$ 680 p/s) and day 10 (2,540 $\pm$ 1,190 p/s). Ten days postinjection, photon counts in the liver steadily decreased and the signal was lost by day 14 (data not shown). The presence of migrated hMSC at day 7 was confirmed by visualizing DiI-labeled hMSC in the sinus space of the liver and the lung parenchyma (Fig. 2C).

In a fully immunocompetent syngeneic host, ffLuc-mMSC isolated from syngeneic Balb/C mice were similarly injected into homeostatic Balb/C mice. Interestingly, the xenograft and syngeneic models followed the same general biodistribution of localizing first to the lung and then residing in the liver, but the timeline of these events was dramatically different (Fig. 2D). ffLuc-mMSC activity in the lungs peaked 1.5 hours postinjection but was not detectable by 18 hours, and instead was found fully distributed to the liver and spleen (Fig. 2E).

hMSC Localization in Cutaneous Wound Models

Without an inflamed microenvironment, infused MSC become undetectable with time. However, in a wounded animal, the MSC localize to and remain at the site of inflammation, in this case puncture wounds and cutaneous incisions. The initial

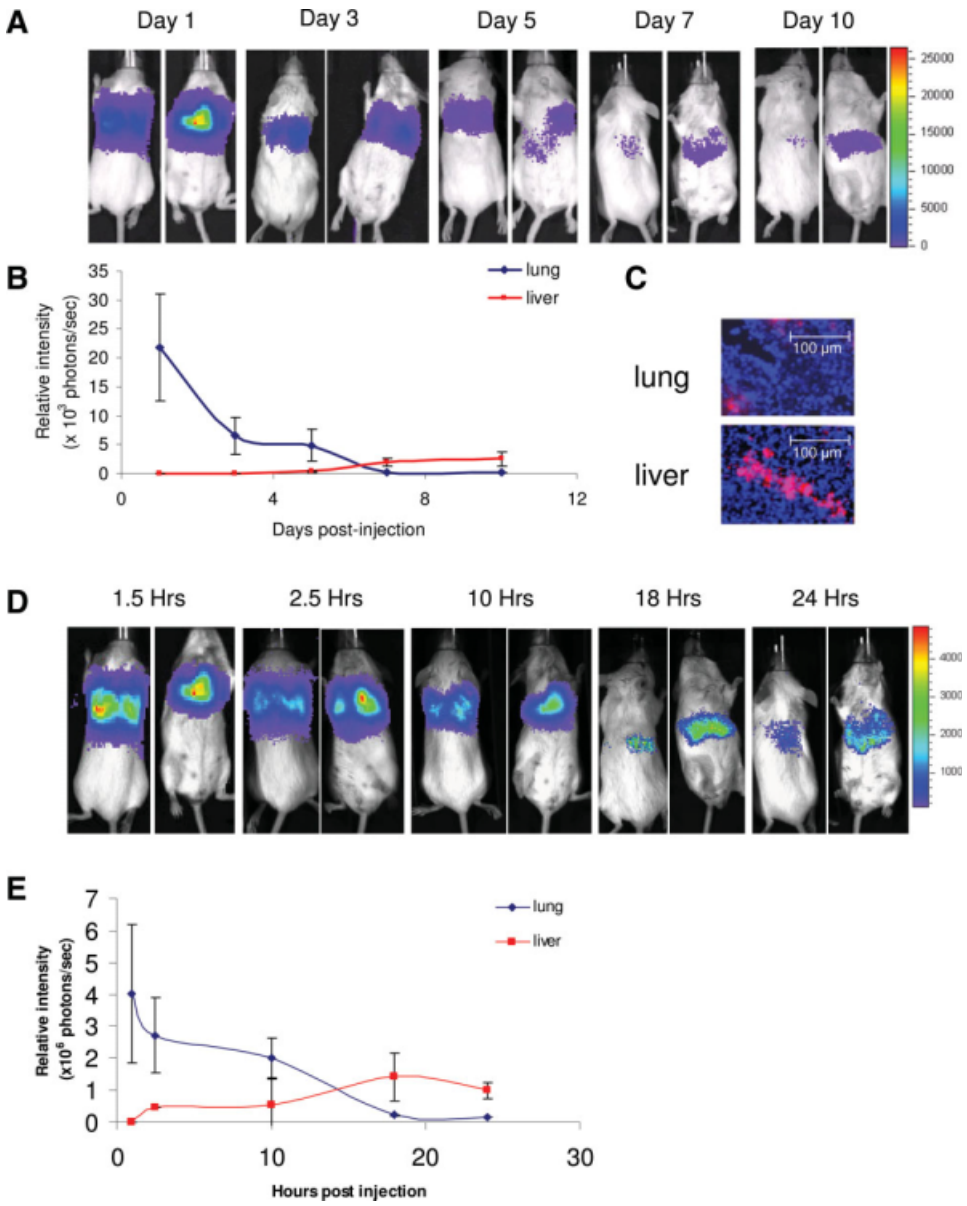

Figure 2. Biodistribution of MSC in homeostatic animals. hMSC were i.v. injected into SCID mice ($n = 5$) and imaged on days 1, 3, 5, 7, and 10 postinjection **(A)**, showing initial localization in the lung and eventual localization in the liver and spleen by day 10. **(B):** Bioluminescent signal was quantified in the lung and liver/spleen regions. **(C):** DiI-labeled hMSC were detected in the liver and lung on day 7 (magnification, 20×). In a syngeneic model, Balb/C ffLuc-mMSC were i.v. injected into homeostatic Balb/C mice ($n = 5$) and imaged 1.5, 2.5, 10, 18, and 24 hours postinjection **(D)**. **(E):** The bioluminescent signal quantified over this time indicated initial mMSC distribution in the lung that had fully migrated to the liver/spleen by 24 hours postinjection. Abbreviations: ffLuc, firefly luciferase; hMSC, human MSC; mMSC, murine MSC; MSC, mesenchymal stromal cell; SCID, severe combined immunodeficient.

observations of MSC tropism for an acute wound were apparent in mice receiving tail vein injections ($n = 5$). ffLuc-hMSC (2.5×10^5) injected on day 1 showed no evidence of luminescent activity in the tail, and all activity was localized to the lungs, as was seen in homeostatic animals. However, by day 3, signal from ffLuc-hMSC (8,910 ± 5,180 p/s) was visible at the sites of three needle punctures in the tail, and activity remained at day 5 (8,610 ± 1,050p/s) (Fig. 3A, 3C). Similar findings were evident in mice that received cutaneous incisions. Three days after surgical incision, 2.5×10^5 ffLuc-hMSC were i.v. injected via the tail vein into the mice (day 0). Mice were imaged three times per week for 2 weeks. In accord with previous findings on day 1, hMSC were found primarily in the lungs. By days 3 and 5, the ffLuc-hMSC signal in the lungs was greatly diminished whereas the signal at the site of the sutured incision was greater (Fig. 3B, 3D). At both of these time points, the bioluminescent signal was significantly higher in animals with lateral incisions than in unwounded controls that received the same MSC doses ($p = .0001$ on day 3 and $p = .0008$ on day 5). The mice were sacrificed after 2 weeks and IHC analysis revealed the presence of the ffLuc$^+$ hMSC incorporated at the site of the cutaneous incisions (Fig. 3E, 3F).

Systemic hMSC Localization in a Xenogeneic MDA-231 Breast Cancer Model

Next, we followed systemic hMSC tropism in an inflamed, tumor microenvironment. ffLuc-hMSC localization was monitored in MDA-231 lung metastasis-bearing mice. Figure 4A shows the ffLuc-hMSC on the day of injection in the lungs, followed by subsequent images on days 3 and 9 showing the cells remaining in the lungs, as well as some dissemination into the liver. On day 29, the final in vivo image was taken before the mice were sacrificed. Quantitation of the bioluminescent signal at days 9 and 29 in tumor-bearing and nontumor-bearing animals, which both received MSC injections, revealed a statistically significant greater signal in tumor-bearing animals ($p = .04$ on day 9 and $p = .02$ on day 27). The lungs, liver, spleen, and kidney were removed and placed in a

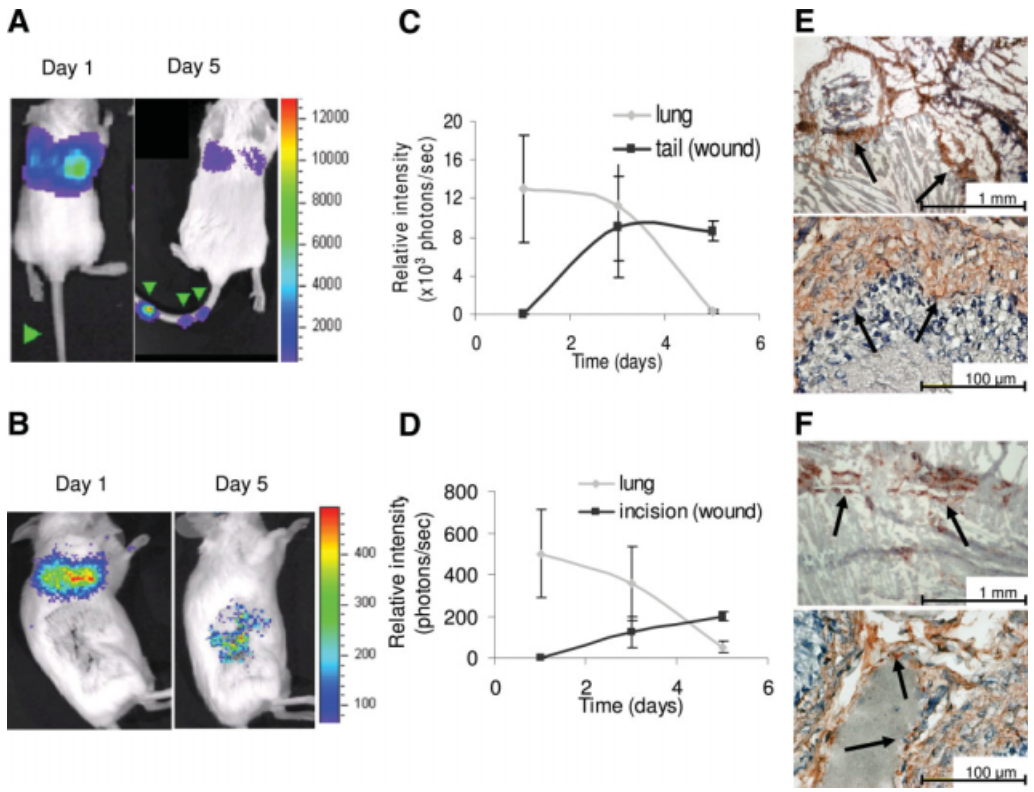

Figure 3. hMSC colocalization in s.c. wound models. ffLuc-hMSC were injected immediately after needle puncture (day 1) or 3 days after surgical incision (day 1). In the needle puncture model, ffLuc-hMSC were injected into SCID mice immediately after wound infliction. Images are shown for representative animals at 1 and 5 days after needle puncture ($n = 5$) **(A)** and after lateral incision ($n = 3$) **(B)**. Bioluminescent activity was quantified on days 1, 3, and 5, demonstrating a decrease in activity in the lung and concurrent increases in activity in the tail wounds **(C)** and cutaneous incisions **(D)**. Immunohistochemistry on sections of tail **(E)** and wounded skin **(F)** demonstrated incorporation of ff-Luc$^+$ hMSC. Abbreviations: ffLuc, firefly luciferase; hMSC, human MSC; MSC, mesenchymal stromal cell; SCID, severe combined immunodeficient.

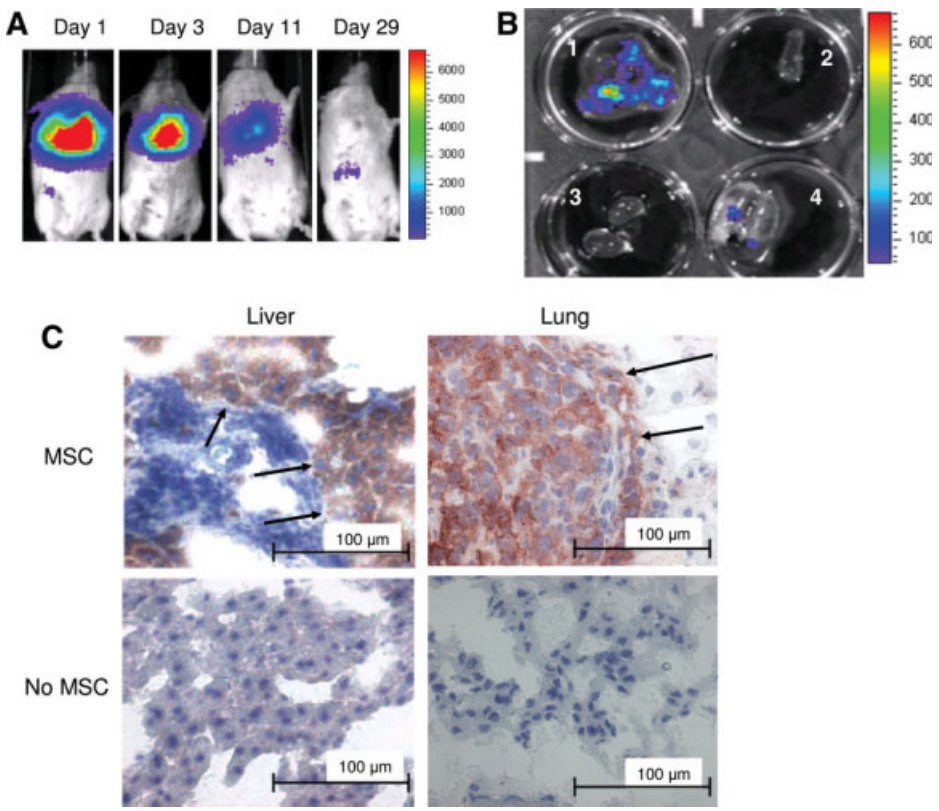

Figure 4. hMSC colocalization with MDA-231 breast cancer in SCID mice. MDA-MB-231 cells were i.v. injected into SCID mice ($n = 5$). Abbreviations: hMSC, human MSC; SCID, severe combined immunodeficient.

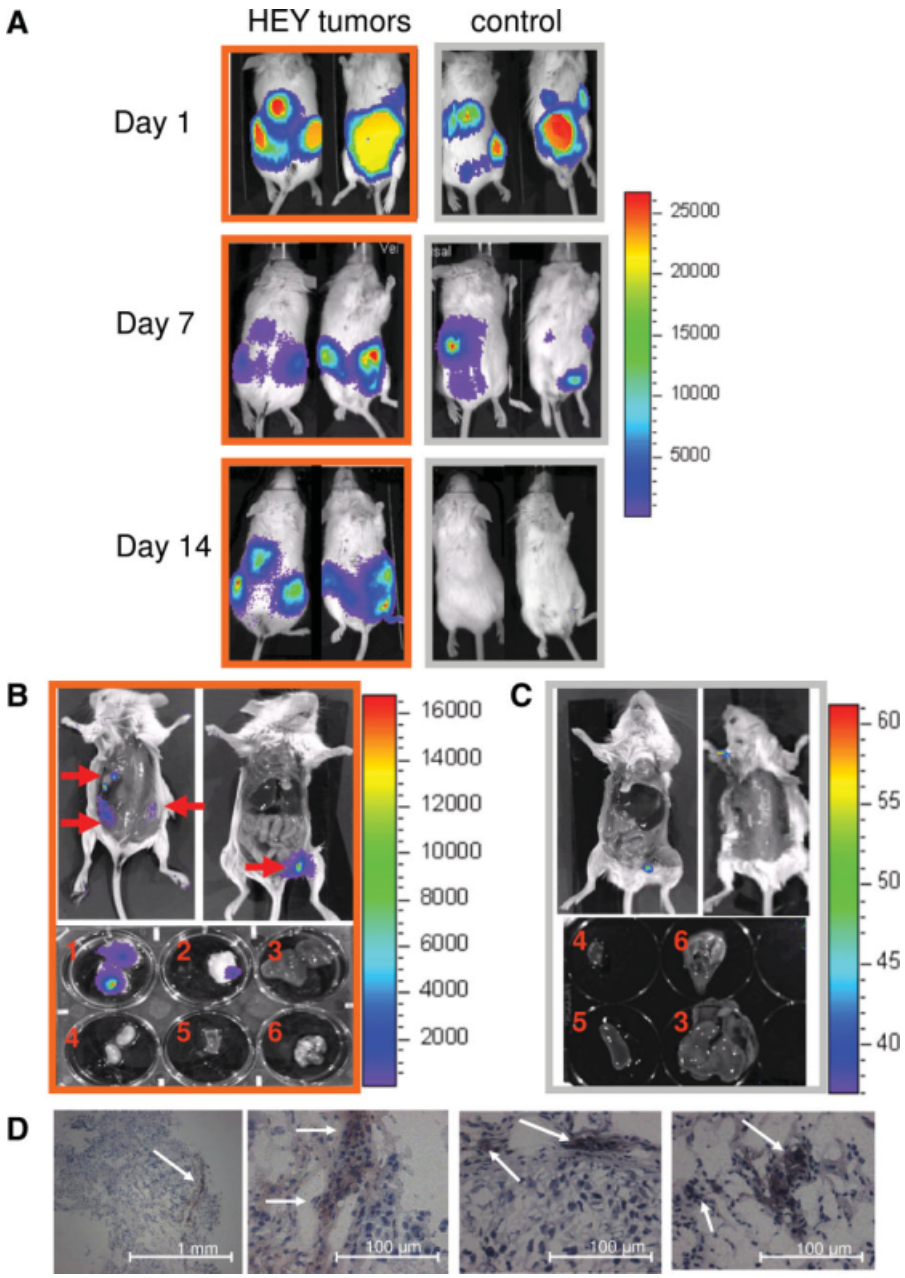

Figure 5. MSC tropism for HEY ovarian carcinoma. SCID mice were i.p. injected with HEY cells ($n = 3$, orange outline) or phosphate-buffered saline ($n = 3$, gray outline). Fifteen days later, ffLuc-hMSC were i.p. injected into tumor-bearing and control mice (day 1). **(A):** Images were acquired at days 1, 7, and 14, indicating initial dissemination throughout the peritoneal cavity, followed by specific localization in tumor-bearing animals and disappearance in control animals. On day 14, the mice were sacrificed and bioluminescent activity was localized to sites of visible tumor development in the open cavities and dissected organs—(1) ventral tumor, (2) dorsal tumor, (3) liver, (4) kidney, (5) spleen, and (6) heart and lungs—of HEY-bearing mice **(B)** but not control mice **(C)**. **(D)** Immunohistochemistry for ffLuc on tumor sections from the HEY-bearing mice confirmed the presence of hMSC (magnification as indicated). Abbreviations: ffLuc, firefly luciferase; hMSC, human MSC; MSC, mesenchymal stromal cell; SCID, severe combined immunodeficient.

six-well plate. The lungs and the liver were both visually positive for tumor nodules that were also positive for ffLuc-hMSC by luminescent imaging (Fig. 4B). IHC was performed on sections of the lung and liver tumor nodules from mice receiving MSC and mice receiving control PBS injection. Anti-ffLuc$^+$ staining is evident only in the lung and liver tumor sections of mice receiving i.v. ffLuc-hMSC injections (Fig. 4C).

i.p.-Injected hMSC Display Tropism for HEY Ovarian Tumors

After establishing selective engraftment of systemically delivered hMSC, we evaluated hMSC tropism for HEY ovarian tumors in a model using i.p.-injected ffLuc-hMSC. Immediately following injection, high levels of ffLuc activity were detected throughout the entire peritoneal cavity (Fig. 5A). Within 3 days, a unique biodistribution pattern emerged, whereby ffLuc-hMSC-generated signals formed distinct punctate regions in the peritoneum. By 7 days postinjection, the overall signal was greatly reduced, revealing three to four hot spots present in the tumor-bearing animals. In the representative animal shown in Figure 5, we observed one hot spot detectable only from the dorsal image in the middle of the back, one hot spot detected only on the ventral image at the top of the left leg, and two hot spots on the sides detected in both images. One region of signal (excluding the injection site) was present in control animals, corresponding to the location of the spleen. Notably, 14 days after ffLuc-hMSC treatment, there was no detectable signal in control animals. In contrast, the tumor-bearing HEY animals had the same hot spots as observed at day 7. The bioluminescent signal quantitated at the tumor site for HEY-bearing animals was significantly greater than that of nontumor-bearing animals, as early as day 3 ($p = .02$). Fourteen days after MSC injection, the animals were sacrificed and the skin was removed to expose

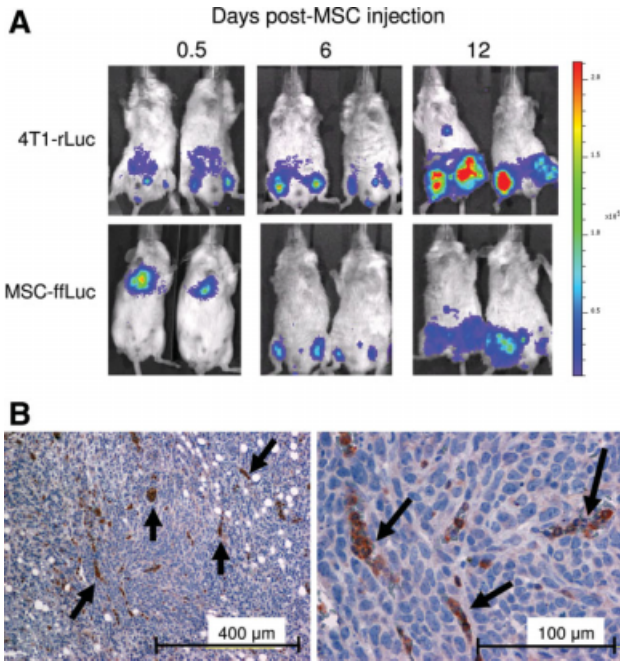

Figure 6. mMSC colocalize with s.c. syngeneic 4T1 murine breast carcinoma. 4T1 cells were s.c. injected into the hind limbs of Balb/C mice ($n = 5$). Ten days after tumor establishment, ffLuc-mMSC were i.v. injected. **(A):** Mice were imaged 0.5, 6, and 12 days after ffLuc-mMSC injection for rLuc (tumor) and ffLuc (mMSC) activities, demonstrating colocalization at days 6 and 12. **(B):** Immunohistochemistry on 4T1 tumor sections revealed incorporation of $ffLuc^+$ MSC. Abbreviations: ffLuc, firefly luciferase; mMSC, murine MSC; MSC, mesenchymal stromal cell; rLuc, renilla luciferase.

organs from the dorsal and ventral perspectives. Three tumors were observed on the dorsal side, and one tumor was visible on the ventral side (identified by red arrows in Fig. 5B). Bioluminescence images acquired localized ffLuc-hMSC activity specifically within these tumor locations (Fig. 5B). Of importance, the anterior tumor had escaped the visceral peritoneal cavity and was established on the outside of the parietal peritoneum, yet it also displayed ffLuc-MSC activity. To confirm localization of the ffLuc-hMSC, the tumors and organs, including heart, lung, kidney, spleen, and liver, were dissected and analyzed separately for bioluminescent signal. As shown in Figure 5B and 5C, only the tumors displayed ffLuc activity, and all organs in both tumor-bearing and control animals were devoid of bioluminescent signal. Additionally, IHC was performed on tumor sections with anti-ffLuc to confirm the presence of ffLuc-hMSC (Fig. 5D).

Systemic mMSC Localization in a Syngeneic s.c. 4T1 Breast Cancer Model

Finally, after observing specific tropism and selective engraftment of hMSC into the xenograft tumor microenvironment, we sought to investigate this behavior in an immunocompetent, syngeneic model. Furthermore, we investigated the tropism of systemically delivered mMSC to an s.c. established breast carcinoma tumor. As previously seen, the ffLuc-mMSC first localized to the lungs, but 6 days after mMSC injection, the ffLuc-mMSC signal colocalized to areas of 4T1-rLuc activity in the s.c. tumors established on the legs (Fig. 6A). Little ffLuc signal was seen in nontumor-bearing animals receiving ffLuc-mMSC injections, and the difference between the two groups was significant at day 6 with a p-value of .0008 and at day 12 with a p-value of .01. Interestingly, as the tumor grew over the next 6 days, indicated by increased rLuc signal at day 12, the ffLuc-MSC signal increased as well (Fig. 6A). IHC performed at this time point on tumor sections revealed positive ffLuc staining (Fig. 6B).

Discussion

We and others have shown that injected MSC engraft into tumor sites and can be used as effective gene delivery vehicles [1, 2, 24]. However, MSC engraftment was evidenced primarily postmortem by IHC and florescent evaluation of tissue sections. Herein, we provide direct bioluminescent evidence of in vivo MSC tropism for and engraftment in multiple inflammatory microenvironments over time. We suggest that these consistent findings of MSC tropism and selective engraftment in multiple tumor and wound models support the possible utility of exogenous MSC as biodetectors of these pathogenic conditions.

A number of studies have demonstrated that exogenously delivered MSC can be found at sites of injury [3–5]. During the wound-healing process, many inflammatory factors, including chemokines, cytokines, growth factors, and extracellular matrices, may regulate the recruitment of MSC to sites of injury. Once at the injured tissue, studies have suggested that MSC aid in wound repair through differentiation into mature cell types, provision of supportive fibrovascular structures including endothelial cells and pericytes, and production of growth factors and cytokines that mediate recovery of injured cells [3–5].

Similar to the wound-repair response, inflammatory cytokines, growth factors, and extracellular matrices play important roles in tumor development and progression. The stroma of malignant tumors closely resembles the granulation tissue of a healing wound [14], and the evidence suggests that solid tumors generate a wound-like environment on their periphery as they apply physical and chemical stress to neighboring tissues. Tumors can therefore be regarded as sites of tissue damage or, according to Dvorak, "wounds that never heal" [14].

In accord with our previous findings, hMSC and mMSC were readily infected with fiber-modified adenovirus and expressed the *ffLuc* reporter gene that was readily detectable by noninvasive imaging [11, 24, 43]. We have shown visualization of as few as 10 s.c.-injected cells, though other reports indicate even lower levels of detection [45], and have demonstrated that larger numbers of cells result in a greater bioluminescent signal. However, the precise quantitation of MSC numbers in tissue-embedded tumors is not possible because of the differing properties of photon absorption and scattering with tissue depth. Therefore, equal bioluminescent signals from s.c.-delivered and i.v.- or i.p.-delivered ffLuc-MSC will not equate to equal cell numbers and are not comparable. Therefore, we can only correlate a higher or lower photon flux to a relatively higher or lower number of MSC present at the wounding site in the same experimental models where tumors are established and MSC are delivered by consistent routes [30].

In noninflamed, immunocompromised SCID mice, i.v.-injected ffLuc-hMSC systemically biodistributed to the lungs first. The hMSC remained lung-resident for 5–7 days, during which time we observed diminished ffLuc signal intensity. After 5–7 days, we observed the much decreased ffLuc-hMSC signal leaving the lungs and arising in the liver and spleen, where it remained detectable until 14 days postinjection. Although the syngeneic, immunocompetent Balb/C model demonstrated a similar pattern of MSC migration, the

period of lung residence was greatly abbreviated. In this model, nearly all ffLuc activity left the lung by 18 hours after ffLuc-mMSC i.v. injection. These cells were then detectable in the liver and spleen for up to 4 weeks.

In both systems, we see an overall decrease in bioluminescent signal from the initial input, which is in accord with findings from other studies [46]. Only metabolically active cells will express the ffLuc reporter; thus, the decrease in bioluminescent signal is representative of a decrease in live (metabolically active) cells. Therefore, we speculate that this initial decrease in photon flux is a result of loss of MSC that may fail to activate critical survival and/or adhesion processes. Most groups investigating stem cell transplantation have reported overall large-scale death of transplanted cells [47, 48], and extensive effort is now being directed toward decreasing lung entrapment [46] and improving conditions for transplanted cell survival [49]. Alternatively, silencing of the *ffLuc* gene could occur, though little evidence of gene silencing occurring within 3–5 days after adenoviral transfection has been published. Furthermore, silencing of >500 copies of the gene product to the point of no detection is unlikely.

Next, to investigate the biodistribution of hMSC in an archetypical, inflamed microenvironment, we generated cutaneous wounds in SCID mice and i.v. injected ffLuc-hMSC. The hMSC began to migrate to the site of the wound after 3 days and remained at the wound for the duration of the experiment. The needle-puncture and sutured wound were both positive for ffLuc-hMSC-generated signal after the initial residence in the lungs. Importantly, this localization was confirmed by IHC for ffLuc at the wounding site, showing incorporation of the MSC into the wounded tissue microenvironment. Of interest, mice were continually monitored for up to 14 days postwounding, and we observed persistent, low levels of ffLuc activity in the region of the wounded tissue even after the wound was completely healed, suggesting that the hMSC became a permanent constituent of the resolved wound site.

After evaluating MSC tropism for wounding events, we investigated this phenomenon in breast and ovarian tumor microenvironments. Irrespective of tumor type, labeled hMSC displayed tropism and selective engraftment within the site(s) of tumor development. In all cases, tumor-bearing animals displayed a statistically significant greater ffLuc bioluminescent signal over the time courses examined when compared with their control, nontumor-bearing counterparts. These findings were consistent, though the immunocompetence of recipient mice, route of MSC administration, and route of tumor establishment differed among experiments. Interestingly, many of the MSC detected by IHC in all acute insult models were found clustered together, perhaps suggesting structural formation by MSC either migrating toward each other or proliferating at the site of inflammation. In support of potential MSC proliferation at the wound site, we previously demonstrated that MSC within the tumor microenvironment incorporate 5-bromo-2′-deoxyuridine, suggesting that tumor-produced mediators can stimulate MSC into proliferation [24] and subsequently contribute to tumor fibrovascular stromal components [50].

As we have previously described, MSC possess an innate tropism for sites of inflammation, including tumors and irradiated environments [2, 11, 24]. Herein, we used bioluminescent imaging to visualize MSC localization to inflamed tissue microenvironments by i.v. and i.p. administration in immunocompetent and immunocompromised mice. Given the specific tropism and selective engraftment of MSC observed under all conditions, one can envision the use of labeled infused MSC as a biodetector possessing an innate tropism for inflammatory-associated chemoattractants as well as inflammatory microenvironments, which could aid in the selection and monitoring of progression of treatment strategies. These important findings acquired through bioluminescent imaging in the lab may readily be transitioned to the clinic through the currently practiced imaging methods of positron emission tomography [40, 51, 52] and magnetic resonance imaging [53–55] that have already been validated for visualization of transplanted MSC.

Acknowledgments

Supported in part by grants from the National Cancer Institute (CA-109451 and Ca-116199 for F.C.M., CA-55164, CA-16672, and CA-49639 for M.A.) and by the Paul and Mary Haas Chair in Genetics (M.A.). S.K. is supported by the Rosalie B Hite Foundation. J.L.D. and F.C.M. are also supported in part by grants from the Susan G Komen Breast Cancer Foundation. E.L.S. is supported in part by the Army Department of Defense (BC083397).

Jennifer Dembinski is currently affiliated with the Norwegian Centre for Stem Cell Research, Institute of Microbiology, Rikshospitalet, Forskningsparken, Gaustadalléen, Oslo, Norway. Martin Dietrich is currently affiliated with the University of Texas Southwestern Medical Center, Dallas, Texas. Michael Weil is currently affiliated with the Department of Environmental and Radiological Health Sciences, Colorado State University, Fort Collins, Colorado.

Disclosure of Potential Conflicts of Interest

The authors indicate no potential conflicts of interest.

References

1 Nakamizo A, Marini F, Amano T et al. Human bone marrow-derived mesenchymal stem cells in the treatment of gliomas. Cancer Res 2005;65:3307–3318.
2 Studeny M, Marini FC, Dembinski JL et al. Mesenchymal stem cells: Potential precursors for tumor stroma and targeted-delivery vehicles for anticancer agents. J Natl Cancer Inst 2004;96:1593–1603.
3 Sasaki M, Abe R, Fujita Y et al. Mesenchymal stem cells are recruited into wounded skin and contribute to wound repair by transdifferentiation into multiple skin cell type. J Immunol 2008;180: 2581–2587.
4 Satake K, Lou J, Lenke LG. Migration of mesenchymal stem cells through cerebrospinal fluid into injured spinal cord tissue. Spine 2004; 29:1971–1979.
5 Neuhuber B, Timothy Himes B, Shumsky JS et al. Axon growth and recovery of function supported by human bone marrow stromal cells in the injured spinal cord exhibit donor variations. Brain Res 2005;1035:73–85.
6 Spaeth E, Klopp A, Dembinski J et al. Inflammation and tumor microenvironments: Defining the migratory itinerary of mesenchymal stem cells. Gene Ther 2008;15:730–738.
7 Murdoch C, Giannoudis A, Lewis CE. Mechanisms regulating the recruitment of macrophages into hypoxic areas of tumors and other ischemic tissues. Blood 2004;104:2224–2234.
8 Okuyama H, Krishnamachary B, Zhou YF et al. Expression of vascular endothelial growth factor receptor 1 in bone marrow-derived mesenchymal cells is dependent on hypoxia-inducible factor 1. J Biol Chem 2006;281:15554–15563.
9 Chen D, Zhang Z, Wu X et al. Distribution of intravenously grafted bone marrow mesenchymal stem cells in the viscera tissues of rats before, after cerebral ischemia. J Clin Rehab Tissue Eng Res 2007;11: 10160–10164.

10 Spitkovsky D, Hescheler J. Adult mesenchymal stromal stem cells for therapeutic applications. Minim Invasive Ther Allied Technol 2008; 17:79–90.
11 Klopp AH, Spaeth EL, Dembinski JL et al. Tumor irradiation increases the recruitment of circulating mesenchymal stem cells into the tumor microenvironment. Cancer Res 2007;67:11687–11695.
12 Mouiseddine M, Fran[cedil]ois S, Semont A et al. Human mesenchymal stem cells home specifically to radiation-injured tissues in a non-obese diabetes/severe combined immunodeficiency mouse model. Br J Radiol 2007;80:S49–S55.
13 Gorin NC, Fliedner TM, Gourmelon P et al. Consensus conference on European preparedness for haematological and other medical management of mass radiation accidents. Ann Hematol 2006;85:671–679.
14 Dvorak HF. Tumors: Wounds that do not heal. Similarities between tumor stroma generation and wound healing. N Engl J Med 1986;315: 1650–1659.
15 Wu Y, Wang J, Scott PG et al. Bone marrow-derived stem cells in wound healing: A review. Wound Repair Regen 2007;15(suppl 1): S18–S26.
16 Saito T, Kuang JQ, Bittira B et al. Xenotransplant cardiac chimera: Immune tolerance of adult stem cells. Ann Thorac Surg 2002;74: 19–24; discussion 24.
17 Orlic D, Kajstura J, Chimenti S et al. Bone marrow cells regenerate infarcted myocardium. Nature 2001;410:701–705.
18 Jackson KA, Majka SM, Wang H et al. Regeneration of ischemic cardiac muscle and vascular endothelium by adult stem cells. J Clin Invest 2001;107:1395–1402.
19 Bittner RE, Schofer C, Weipoltshammer K et al. Recruitment of bone-marrow-derived cells by skeletal and cardiac muscle in adult dystrophic mdx mice. Anat Embryol (Berl) 1999;199:391–396.
20 Horwitz EM, Prockop DJ, Fitzpatrick LA et al. Transplantability and therapeutic effects of bone marrow-derived mesenchymal cells in children with osteogenesis imperfecta. Nat Med 1999;5:309–313.
21 Hofstetter CP, Schwarz EJ, Hess D et al. Marrow stromal cells form guiding strands in the injured spinal cord and promote recovery. Proc Natl Acad Sci U S A 2002;99:2199–2204.
22 Bacigalupo A. Management of acute graft-versus-host disease. Br J Haematol 2007;137:87–98.
23 Kidd S, Spaeth E, Klopp A et al. The (in) auspicious role of mesenchymal stromal cells in cancer: Be it friend or foe. Cytotherapy 2008; 10:657–667.
24 Studeny M, Marini FC, Champlin RE et al. Bone marrow-derived mesenchymal stem cells as vehicles for interferon-beta delivery into tumors. Cancer Res 2002;62:3603–3608.
25 Allers C, Sierralta WD, Neubauer S et al. Dynamic of distribution of human bone marrow-derived mesenchymal stem cells after transplantation into adult unconditioned mice. Transplantation 2004;78:503–508.
26 Pereira RF, Halford KW, O'Hara MD et al. Cultured adherent cells from marrow can serve as long-lasting precursor cells for bone, cartilage, and lung in irradiated mice. Proc Natl Acad Sci U S A 1995;92: 4857–4861.
27 de Wet JR, Wood KV, Helinski DR et al. Cloning of firefly luciferase cDNA and the expression of active luciferase in *Escherichia coli*. Proc Natl Acad Sci U S A 1985;82:7870–7873.
28 Contag CH, Jenkins D, Contag PR et al. Use of reporter genes for optical measurements of neoplastic disease in vivo. Neoplasia 2000;2:41–52.
29 Contag CH, Spilman SD, Contag PR et al. Visualizing gene expression in living mammals using a bioluminescent reporter. Photochem Photobiol 1997;66:523–531.
30 Contag CH, Bachmann MH. Advances in in vivo bioluminescence imaging of gene expression. Annu Rev Biomed Eng 2002;4:235–260.
31 Sweeney TJ, Mailänder V, Tucker AA et al. Visualizing the kinetics of tumor-cell clearance in living animals. Proc Natl Acad Sci U S A 1999;96:12044–12049.
32 Edinger M, Sweeney TJ, Tucker AA et al. Noninvasive assessment of tumor cell proliferation in animal models. Neoplasia 1999;1:303–310.
33 Azadniv M, Dugger K, Bowers WJ et al. Imaging $CD8^+$ T cell dynamics in vivo using a transgenic luciferase reporter. Int Immunol 2007;19:1165–1173.
34 Wang X, Rosol M, Ge S et al. Dynamic tracking of human hematopoietic stem cell engraftment using in vivo bioluminescence imaging. Blood 2003;102:3478–3482.
35 Cao YA, Wagers AJ, Beilhack A et al. Shifting foci of hematopoiesis during reconstitution from single stem cells. Proc Natl Acad Sci U S A 2004;101:221–226.
36 Min JJ, Ahn Y, Moon S et al. In vivo bioluminescence imaging of cord blood derived mesenchymal stem cell transplantation into rat myocardium. Ann Nucl Med 2006;20:165–170.
37 van der Bogt KE, Sheikh AY, Schrepfer S et al. Comparison of different adult stem cell types for treatment of myocardial ischemia. Circulation 2008;118(14 suppl):S121–S129.
38 van der Bogt KE, Schrepfer S, Yu J et al. Comparison of transplantation of adipose tissue- and bone marrow-derived mesenchymal stem cells in the infarcted heart. Transplantation 2009;87:642–652.
39 Tögel F, Yang Y, Zhang P et al. Bioluminescence imaging to monitor the in vivo distribution of administered mesenchymal stem cells in acute kidney injury. Am J Physiol Renal Physiol 2008;295: F315–F321.
40 Love Z, Wang F, Dennis J et al. Imaging of mesenchymal stem cell transplant by bioluminescence and PET. J Nucl Med 2007;48: 2011–2020.
41 Hwang do W, Jang SJ, Kim YH et al. Real-time in vivo monitoring of viable stem cells implanted on biocompatible scaffolds. Eur J Nucl Med Mol Imaging 2008;35:1887–1898.
42 Ling X, Konopleva M, Zeng Z et al. The novel triterpenoid C-28 methyl ester of 2-cyano-3, 12-dioxoolen-1, 9-dien-28-oic acid inhibits metastatic murine breast tumor growth through inactivation of STAT3 signaling. Cancer Res 2007;67:4210–4218.
43 Yotnda P, Zompeta C, Heslop HE et al. Comparison of the efficiency of transduction of leukemic cells by fiber-modified adenoviruses. Hum Gene Ther 2004;15:1229–1242.
44 Dominici M, Le Blanc K, Mueller I et al. Minimal criteria for defining multipotent mesenchymal stromal cells. The International Society for Cellular Therapy position statement. Cytotherapy 2006;8:315–317.
45 Rabinovich BA, Ye Y, Etto T et al. Visualizing fewer than 10 mouse T cells with an enhanced firefly luciferase in immunocompetent mouse models of cancer. Proc Natl Acad Sci U S A 2008;105:14342–14346.
46 Fischer UM, Harting MT, Jimenez F et al. Pulmonary passage is a major obstacle for intravenous stem cell delivery: The pulmonary first-pass effect. Stem Cells Dev 2009;18:683–692.
47 Mooney DJ, Vandenburgh H. Cell delivery mechanisms for tissue repair. Cell Stem Cell 2008;2:205–213.
48 Daley GQ, Scadden DT. Prospects for stem cell-based therapy. Cell 2008;132:544–548.
49 Copland IB, Lord-Dufour S, Cuerquis J et al. Improved autograft survival of mesenchymal stromal cells by plasminogen activator inhibitor 1 inhibition. Stem Cells 2009;27:467–477.
50 Spaeth EL, Dembinski JL, Sasser AK et al. Mesenchymal stem cell transition to tumor-associated fibroblasts contributes to fibrovascular network expansion and tumor progression. PLoS One 2009;4: e4992.
51 Mayer-Kuckuk P, Doubrovin M, Bidaut L et al. Molecular imaging reveals skeletal engraftment sites of transplanted bone marrow cells. Cell Transplant 2006;15:75–82.
52 Hung SC, Deng WP, Yang WK et al. Mesenchymal stem cell targeting of microscopic tumors and tumor stroma development monitored by noninvasive in vivo positron emission tomography imaging. Clin Cancer Res 2005;11:7749–7756.
53 Bos C, Delmas Y, Desmoulière A et al. In vivo MR imaging of intravascularly injected magnetically labeled mesenchymal stem cells in rat kidney and liver. Radiology 2004;233:781–789.
54 Wu X, Hu J, Zhou L et al. In vivo tracking of superparamagnetic iron oxide nanoparticle-labeled mesenchymal stem cell tropism to malignant gliomas using magnetic resonance imaging. Laboratory investigation. J Neurosurg 2008;108:320–329.
55 Amsalem Y, Mardor Y, Feinberg MS et al. Iron-oxide labeling and outcome of transplanted mesenchymal stem cells in the infarcted myocardium. Circulation 2007;116(11 suppl):I38–I45.

See www.StemCells.com for supporting information available online.